Final Draft

of the original manuscript

Li, Y.; Pyczak, F.; Stark, A.; Wang, L.; Oehring, M.; Paul, J.; Lorenz, U.:
Temperature dependence of misfit in different Co–Al–W ternary alloys measured by synchrotron X-ray diffraction.
In: Journal of Alloys and Compounds. Vol. 819 (2020) 152940.

First published online by Elsevier: 07.11.2019

https://dx.doi.org/10.1016/j.jallcom.2019.152940

Temperature dependence of misfit in different Co-Al-W ternary alloys measured by synchrotron X-ray diffraction

Yuzhi Li[a*], Florian Pyczak[b], Andreas Stark[b], Li Wang[b*], Michael Oehring[b], Jonathan Paul[b], Uwe Lorenz[b]

a. College of Mechanical and Electrical Engineering, Shaanxi University of Science and Technology, Xi'an 710021, China

b. Institute of Materials Research, Helmholtz-Zentrum Geesthacht, 21502 Geesthacht, Germany

Corresponding author: liyuzhi@sust.edu.cn **(Yuzhi Li)**;

Li.wang1@hzg.de **(Li Wang)**

Abstract

The lattice misfit between the γ matrix and coherently embedded γ′ precipitates in the ternary system Co-9Al-xW-0.1B(x=8,9,11) was measured in-situ by synchrotron X-ray diffraction between room temperature and 1000 °C. The lattice parameters of both γ′ and γ phases increase with rising temperature. The thermal expansion of both phases is similar before the γ′ precipitates start to dissolve. When the temperature rises above 700°C, the lattice parameter of the γ phase increases more rapidly due to a redistribution of W atoms from the dissolving γ′ precipitates. Thus, the misfit remains almost constant in the temperature range between 20 °C and 700 °C but decreases drastically above 700 °C. Nevertheless, the misfit in these Co-Al-W alloys remains positive up to the γ′ solvus.

Keywords: misfit, synchrotron X-ray diffraction, thermal expansion, element re-distribution

Introduction

That $L1_2$ precipitates (γ′ phase) are present in the ternary system Co-Al-W was most probably first discovered by Lee[1]. After a publication of Sato et al.[2], it gained broader interest and such alloys have been intensively studied recently with respect to their microstructure and hardening mechanisms[3-6]. With a solvus temperature of the $L1_2$ precipitate phase of up to 1000 °C and a high volume fraction of γ′ phase embedded as coherent particles in a γ matrix, this novel type of Co-base alloys presents equal or even superior high temperature mechanical properties compared to some γ′ hardened Ni-base superalloys[7-9]. Even the thermal stability of the γ′ phase in these Co-Al-W ternary alloys are not excellent enough at high temperatures[3], it can be improved to some

extent by adding elements such as Ni, Ti, Ta and so on[10]. The additional elements also increase the volume fraction and γ′ solvus temperatures, which makes the Co-Al-W-base alloys more competitor to Ni-base superalloys on mechanical properties at elevated temperature[10]. The γ′ particles are frequently of cubic shape and aligned along <001> directions, showing the initial orientation relationship of $\{001\}_{\gamma'}||\{001\}_{\gamma}$ and $<100>_{\gamma'}||<100>_{\gamma}$. Small differences in the unit cell sizes of γ, with fcc lattice structure, and γ′, with $L1_2$ structure, result in a lattice misfit between the two, which is defined as $\delta = 2(a_{\gamma'} - a_{\gamma})/(a_{\gamma'} + a_{\gamma})$, where $a_{\gamma'}$ and a_{γ} represent the lattice parameters of γ′ and γ phases. The high mechanical strength is caused primarily by the morphology and fraction of the γ′ precipitates[11], but their shape and coherency state both change during service at high temperature under external stress, which is mainly caused by the misfit stresses[12,13].

It is well known that coherency stresses and strains exist in both phases, especially near the boundaries between the cubic γ′ precipitates and the γ matrix, which can significantly influence the morphology, thermal stability and orientation of γ′ precipitates[14,15]. Moreover, post-crept microstructure of the alloys particularly depends on the value and the sign of the misfit at high temperature[16]. The alloys during creep frequently exhibit a directional coarsening of the precipitates along one or two of the <001> directions resulting in rod or plate-like precipitates. This process is- called rafting. The sign of the misfit determines the rafting direction being either perpendicular (negative misfit) or parallel (positive misfit) to the applied stress for tensile creep. For compressive creep stress the situation is reversed[17].

Due to the small differences between the lattice constants of γ and γ′ phase which may further reduced because the coherency results in a constraint of the lattice constants in both phases, it is difficult to measure the misfit. In normal X-ray diffraction (XRD), the reflections of the γ and γ′ phases normally overlap to some extent and are hard to separate[18]. Convergent beam electron diffraction (CBED) by transmission electron microscopy (TEM) is an alternative method to measure the lattice constants and by this the misfit. Nevertheless, it is a local method and the high complexity of the measurements makes it prohibitive to acquire enough measurement results from different locations to determine the average misfit of an alloy with sufficient statistical significance[19]. In addition, CBED is performed in a thin TEM foil which may alter the misfit due to relaxation of the lattice. By chemically dissolving either the γ′ precipitates or the γ matrix it is possible to determine the lattice parameters of both phases separately by XRD. It is advantageous that this method provides the lattice parameters under unconstrained conditions which are difficult to access by other methods. Nevertheless, the chemical dissolution can lead to changes in the

elemental composition of both phases, which can cause erroneous results[20]. Time-of-flight neutron scattering technique can provide higher intensity for superlattice reflections and is able to transmit further through dense materials[21]. However, the measurement by neutron takes longer recording time, due to its lower beam flux[22].Using synchrotron generated X-rays to measure the lattice constants and misfit has a number of advantages because their energy and intensity are higher by one order of magnitude compared to lab X-ray sources. It is possible to measure in transmission, which minimizes the detrimental effects of oxidation or near surface element depletion during high temperature measurements. In addition, due to the high intensity and low background superlattice reflections, which represent the lattice constant of the ordered γ′ phase alone but are normally weak can be measured and used as an additional information to deconvolute the combined γ/γ′ fundamental reflections.

At present, rather limited measurements have been conducted on the room temperature lattice misfit and especially on the temperature dependence of the misfit of these novel Co-base superalloys. This is an undesirable situation for further investigation of the creep deformation mechanisms and morphological stability of the γ′ phase at high temperature, which both strongly depend on the misfit. The creep behavior of Co-Al-W single crystal alloys has been investigated systematically at 850 °C[5,23]. However, the driving force for rafting, caused by combination of coherency stress due to the γ/γ′ misfit and externally applied stress, was not discussed in detail. The partitioning of alloying elements may change the thermal expansion and lattice constants with temperature and thus influence the misfit and mechanical properties[8]. This misfit evolution is also important for the composition improving of the novel Co-Al-W-base superalloys. Therefore, three Co-Al-W ternary alloys with different tungsten content Co-9Al-xW-0.1B(x=8,9,11) were investigated in this study with respect to the temperature dependence of their γ/γ′ misfit during heating from room temperature to 1000 °C.

Experiments

Material and heat-treatment

The investigated alloys Co-9Al-8W-0.1B, Co-9Al-9W-0.1B, Co-9Al-11W-0.1B (all atomic percent) were produced in a vacuum arc melting furnace. For the sake of brevity, these alloys will be termed as 8W, 9W and 11W. The ingots were melted 5 times into 64g buttons to ensure chemical homogeneity. The small amount of boron was added in the alloys to strengthen the grain boundaries[4,24].

The solution heat-treatment was conducted at 1300°C for 12 hours under vacuum. The temperatures for the solution heat treatment were based on the melting points and γ′ solvus temperatures reported in[4]. Subsequent aging treatments were performed at 900 °C for 200 hours in air and the specimens were cooled in air.

Synchrotron X-ray diffraction

The polycrystalline samples were cut by spark erosion into cylinders with a height of 8 mm and a diameter of 5.5 mm. The in-situ synchrotron X-ray diffraction experiments were carried out at the Helmholtz-Zentrum Geesthacht operated High Energy Materials Science (HEMS) beamline at the PETRA III storage ring of Deutsches Elektronen-Synchrotron (DESY) in Hamburg. In order to penetrate the specimen, high-energy X-rays with a photon energy of 100 keV (corresponding to a wavelength of 0.0124 nm) and a beam cross-section of 1×1 mm^2 were used. The resulting Debye–Scherrer diffraction patterns/rings were continuously recorded on a Mar555 flat panel detector with an exposure time of 0.1 s. A standard lanthanum hexaboride (LaB_6) powder specimen was used for a calibration measurement to determine the instrumental parameters, such as the specimen-detector distance and beam center. The Debye-Scherrer diffraction rings were azimuthally integrated using the FIT2D software (ESRF, Grenoble, France)

All three alloys were analysed during heating using 50 °C steps from room temperature up to 850 °C and then 25°C steps up to 1000°C. The specimens were isothermally held at each temperature for 15 minutes to ensure sufficient heat transfer and to attain equilibrium conditions. The temperature was controlled by a thermocouple directly spot-welded onto the specimen. An induction furnace was used for heating and the measurements were carried out under an argon atmosphere. The in-situ diffraction information was recorded every 30 seconds during the heating process.

Diffraction peak fitting

The diffraction patterns collected on the 2D detector were azimuthally integrated to generate the intensity over 2θ plots of the peaks which were further processed. The grains in the specimen were bigger than 1μm and thus less than 5 grains took part in the diffraction. Moreover, in one grain, the γ and γ′ phases are arranged in the same crystallographic orientation. As a result, the diffraction spots of the γ and γ′ phases on the 2D-detector are located in very well defined azimuthal ranges. Thus, they can be integrated without including contributions from the Co_3W or CoAl phase because those - especially the Co_3W phase at grain boundaries - were arranged in different

crystallographic orientations[3]. Therefore, by integrating the appropriate azimuthal and 2θ ranges the influence of others phases except γ/γ′ can almost be excluded.

To separate the overlapped γ/γ′ diffraction peaks, the software package XPLOT (ESRF Grenoble, France) was utilized to fit the overall profile with two single peaks using a Pseudo-Voigt function that consists of a Gaussian and a Lorentzian function. The lattice constant of γ′ was determined by fitting a superlattice reflection which is scattered only from the ordered γ′ phase. Subsequently, an asymmetric fundamental reflection containing combined γ/γ′ contributions was fitted using two Pseudo-Voigt functions. This procedure was automatically performed by the XPLOT program after manually fixing the peak position of the γ′ phase at the value determined from the superlattice reflection. The misfit was calculated from the lattice constants of the phases γ and γ′ phases, according to the definition given above.

Results and discussion

Microstructure characterization

The microstructures of the three alloys after solution and ageing heat-treatment are shown in Fig. 1. The corresponding selected area diffraction patterns from the [001] zone axis are shown together with the TEM and SEM micrographs. It is evident that the γ′ precipitates are arranged parallel to <001> orientations as expected. The average edge length of γ′ precipitates varies from 150 nm to 320 nm in the three alloys, and the volume fraction of γ′ phase is in the range of 43% to 85%, both increasing with W content. It is notable that the morphology of the γ′ precipitates in 11W appears to be more cuboidal. Secondary γ′ precipitates are visible in the TEM micrographs of 8W and 9W, which has already been reported in the authors' earlier study[3]. In this study, the effects of secondary γ′ precipitates are not considered in detail because their extremely low volume fraction and small size make their influence on the overall diffraction signal from the primary γ′ particles and the γ matrix negligible. Moreover, the Co_3W-$D0_{19}$ phase is present at grain boundaries as shown in Fig.1(a4-c4). But their diffraction peaks are much weaker compared to the γ/γ′ phases. Co_3W-$D0_{19}$ phase in the grain interior and CoAl-B2 phases if present at all were too few to be detected by BSE and XRD after 200h ageing, but were found after 2000h of ageing[3].

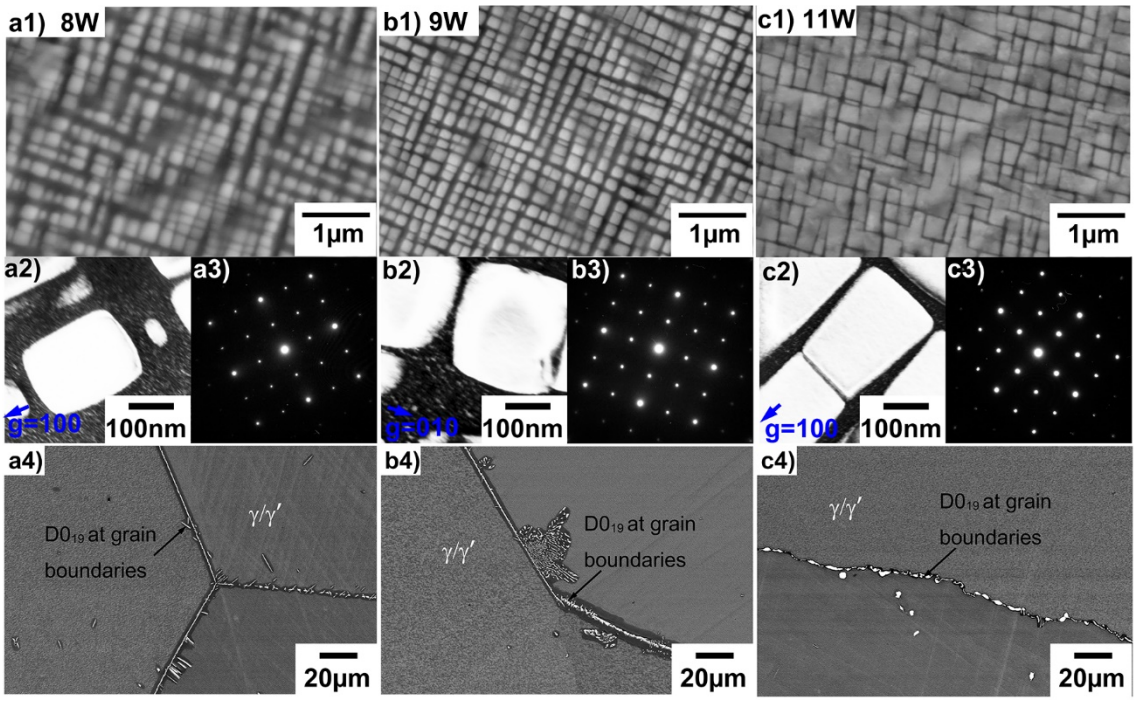

Fig. 1 (a1-c1) BSE images of the γ/γ′ microstructure after ageing at 900°C for 200 h; (a2-c2) Dark field TEM micrographs taken along <001> with (010) diffraction; (a3-c3) SADPs; (a4-c4) BSE images of the $D0_{19}$ phase at grain boundaries.

Lattice parameter of γ′ phase derived from superlattice peaks

Fig.2 shows the temperature evolution of the (110) diffraction peak profiles for the 8W alloy. If this superlattice reflection was fitted with only one Pseudo-Voigt function, a significant margin remained at the shoulder. Therefore, the peak was fitted using two peaks: a sharp larger one and a broad smaller one as illustrated in Fig.2a, b. The large peak was regarded as the diffraction of the primary cuboidal γ′ phase, which is labelled as γ′ and plotted as a blue line. The broader sub-peak is assumed to belong to regions of the γ′ particles distorted by the internal coherency stress within the γ′ particles which exists near the γ/γ′ interfaces. It is labelled as γ′-sub and plotted as a green line. The red line was obtained by summing up these two fitted peaks, and the black dots represent the actual values measured by HEXRD.

Both, the large peak and the small peak shifted to lower diffraction angles during the heating process. Nevertheless, the small peak is always located at slightly higher diffraction angles than the primary γ′ peak at all temperatures. As the temperature increased, the decrease of the sub-peak area (the green peak shown in Fig.2c) suggests that the effect from the coherency stresses vanishes gradually as the temperature increases. The weakening of the overall diffraction in the profile

recorded at 925 °C, and shown in Fig.2d, stems from the dissolution of γ′ precipitates and agrees with the onset of γ′ dissolution in 8W at 920 °C determined by DSC[4]. At temperatures above 925 °C no γ′ superlattice reflections were detected in 8W anymore as the γ′ phase has completely dissolved.

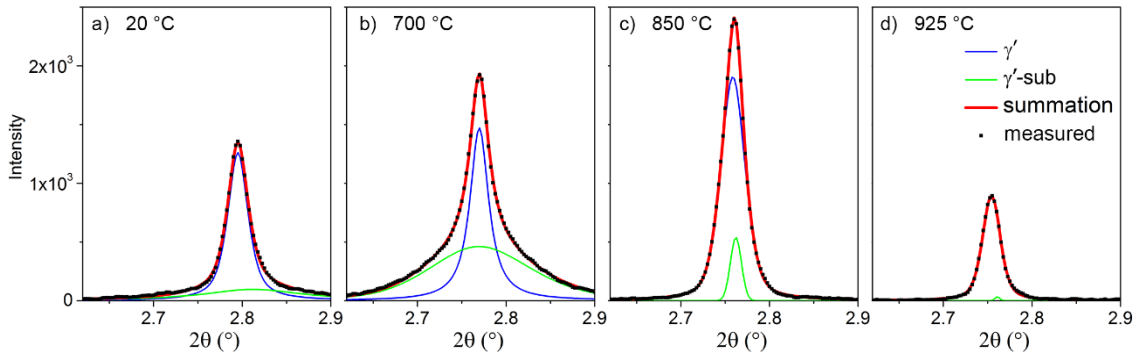

Fig.2 (110) superlattice peaks of 8W recorded at different temperatures and fitted by two γ′ sub-peaks - (a) 20 °C; (b) 700 °C; (c) 850 °C; (d) 925 °C.

The (110) superlattice diffraction of the 9W alloy was also deconvoluted into two sub-peaks as shown in Fig.3. The primary γ′ precipitates are represented by the blue higher peak and the existence of the small green sub-peak was also regarded as being caused by the effect from the coherency stresses at the γ/γ′ interfaces. As was the case in 8W, the two sub-peaks shifted to lower diffraction angles with rising temperature due to the thermal expansion of the lattices. Both diffraction peaks diminished significantly after reaching 900°C and disappeared eventually at 975°C, due to the dissolution of the γ′ precipitates.

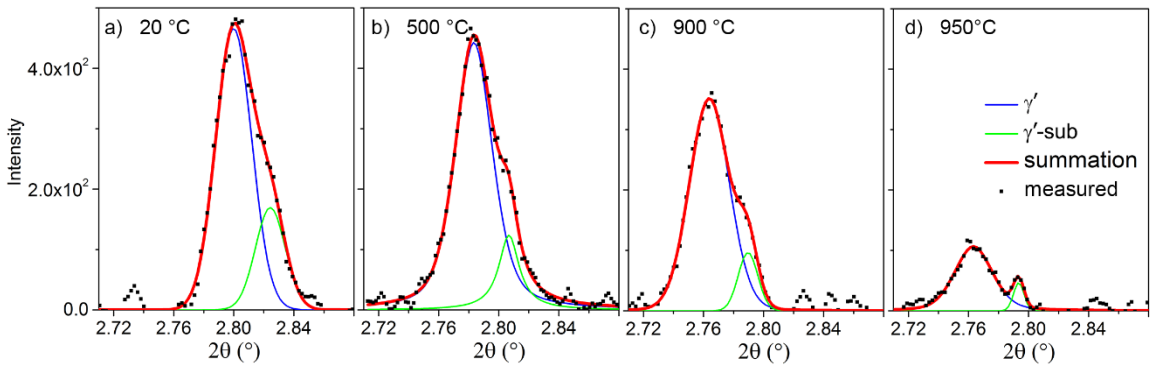

Fig.3 The (110) superlattice peaks of 9W recorded at different temperatures and fitted by two γ′ sub-peaks - (a) 20 °C; (b) 500 °C; (c) 900 °C; (d) 950 °C.

The asymmetric (001) diffraction profiles of 11W at different temperatures are shown in Fig.4. The main peak in blue represents the undistorted volume of the γ′ precipitates while the sub-

peak in green was induced by the distortion of the γ′ phase at the γ/γ′ interfaces. Both peaks continuously shift to lower diffraction angles with increasing temperature similar to the situation found in the alloys 8W and 9W. At 1000 °C the superlattice reflection is nearly undetectable in accordance with the γ′ solvus temperature of 11W, which was determined to lie between 974°C and 1049°C by DSC[4]. The separation of the peaks representing the undistorted and distorted volume of the γ′ precipitates does not change significantly until the dissolution of γ′ precipitates.

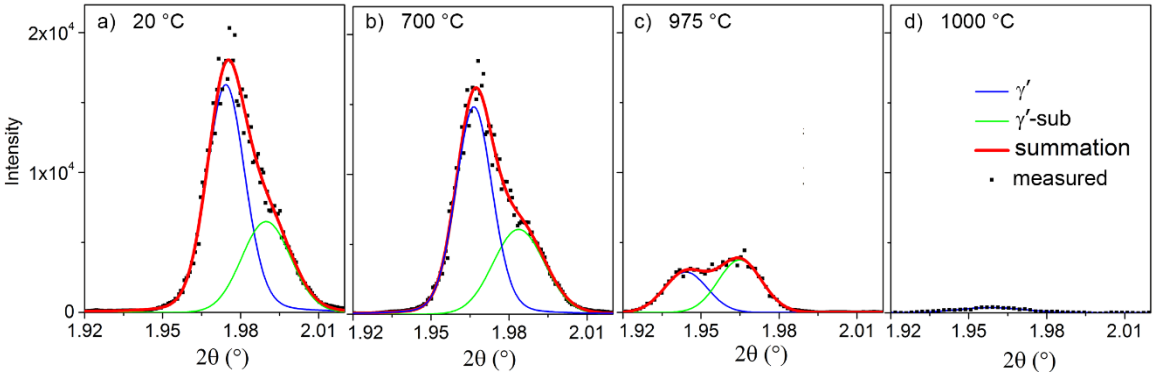

Fig.4 The (001) superlattice peaks of 11W recorded at different temperatures and fitted by two γ′ sub-peaks - (a) 20 °C; (b) 700 °C; (c) 975 °C; (d) 1000 °C.

The lattice parameters of the γ′ phase of all three alloys derived from the different superlattice reflections differ slightly, as shown in Fig.5 The lattice parameters belonging to the main peaks are presented. The lattice parameters of the γ′ phase as shown in Fig.5 were determined by averaging over the superlattice reflections such as (001), (011), (012), (003), (123) and (112) to increase the accuracy.

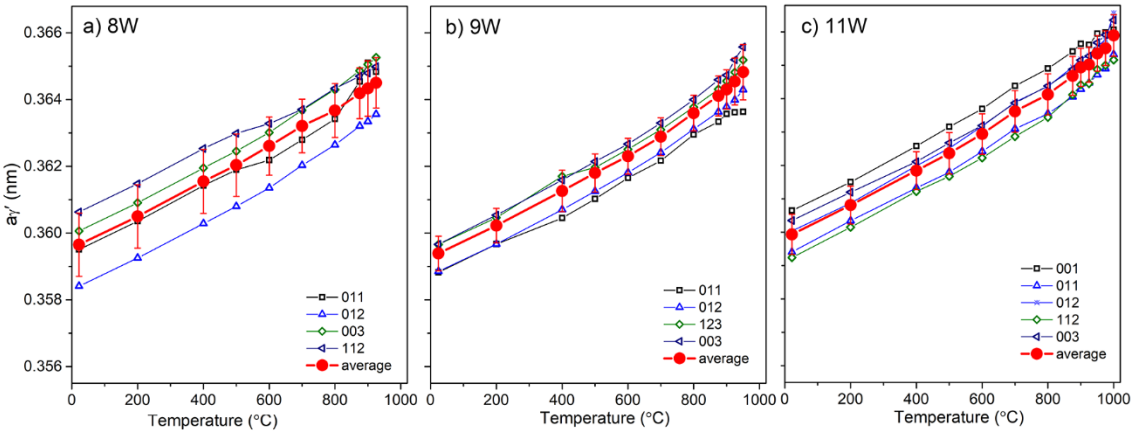

Fig.5 The lattice parameters of γ′ phase derived from individual reflections and the average value.

Lattice parameter of γ phase derived from deconvolution of fundamental peaks

The lattice parameters of the γ phase were determined from the deconvolution of one fundamental diffraction peak into two sub-peaks: one belonging to the γ′ precipitate phase and the other to the γ matrix phase. For the sub-peak of the γ′ phase the average lattice parameters determined from the superlattice reflections were used. The peak position of γ′ precipitates was fixed at that value and the other sub-peak was regarded as diffraction of the γ matrix.

Examples of the split profiles of the (220) diffraction peaks of the 8W alloy at different temperatures are shown in Fig. 6. Both peaks shifted towards lower diffraction angles with rising temperature. The peaks of γ phase shifted faster towards lower diffraction angles than those of the γ′ phase at temperatures higher than 700 °C. This could indicate that the thermal expansion of the γ matrix phase is larger at those temperatures. Nevertheless, such an effect could also be caused by the beginning dissolution of the γ′ phase. The alloying elements initially being contained in the γ′ phase are redistributed to the γ matrix and increase its lattice parameter[25,26]. Thus, the observed behavior could be caused by differences in thermal expansion coefficients, redistribution of alloying elements between γ′ and γ phase or a combination of both. Meanwhile, the intensity of all peaks decreased continuously during heating. The overall profile decreases in intensity, but the separation of the γ and γ′ sub-peaks stays constant below 700 °C, while both sub-peaks tend to merge into a more symmetric overall profile afterwards, due to the higher increase of the γ lattice constant. The intensity of the sub-peaks of the γ′ phase decreases more strongly than the one of the γ phase most probably because of the dissolution of the γ′ phase at elevated temperature.

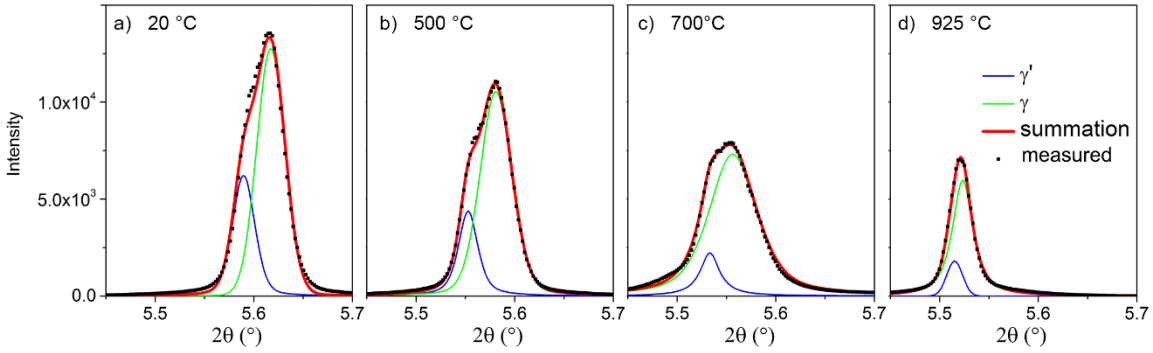

Fig.6 The (220) fundamental reflection of alloy 8W together with the fitted sub-peaks of the phases γ and γ′ at different temperatures: (a) 20 °C; (b) 500 °C; (c) 700 °C; (d) 925°C.

The overall profiles of the (220) reflection of the 9W alloy and the sub-peaks of the γ and γ′ phases are shown in Fig. 7. It is notable that the intensity of the γ′ phase here is much weaker than

that of the γ phase. It is not clear why the relative intensity of the sub-peak of the γ phase from the (220) diffraction is much higher. However it is noteworthy that a similar difference between the heights of γ′ and γ sub-peaks exists when deconvoluting the (111) fundamental peak. Thus, it can be ruled out that this is just a peculiarity of the (220) peak. The peak position of the γ phase is always located at higher diffraction angles than the one of the γ′ phase which is also not affected by the thermal expansion with increasing temperature.

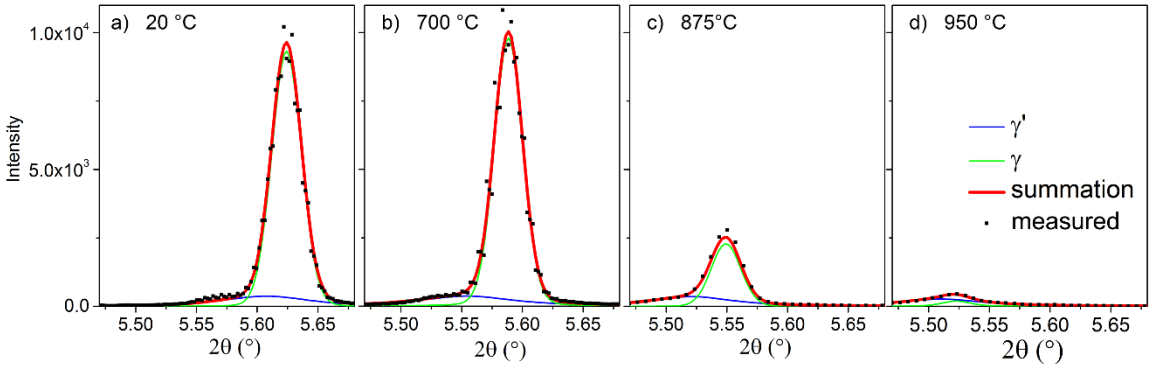

Fig.7 The (220) fundamental reflection of alloy 9W together with the fitted sub-peaks of the phases γ and γ′ at different temperatures: (a) 20 °C; (b) 700 °C; (c) 875 °C; (d) 950°C.

The evolution of the (111) diffraction peak for the alloy 11W is shown in Fig. 8 together with the sub-peaks of the γ and γ′ phases determined by the fitting procedure. The sub-peak of the γ′ precipitates is always located at lower diffraction angles or, in other words, higher lattice parameters than the sub-peak of the γ phase. This is maintained while both sub-peaks shift to lower diffraction angles during the heating due to the thermal expansion. The overall peak intensity and the intensity of sub-peaks both decrease with increasing temperature, similar to the situation in the alloy 8W. A symmetric overall profile is only found at a higher temperature of 975 °C due to the higher γ′ solvus temperature of the alloy 11W, as well as the high γ′ volume fraction in this alloy.

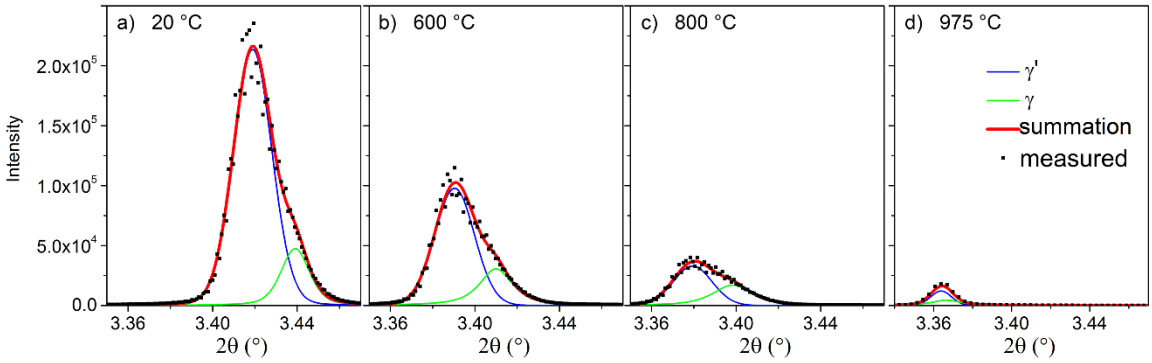

Fig.8 The (111) fundamental reflection of alloy 11W together with the fitted sub-peaks of the phases γ and γ′ at different temperatures: (a) 20 °C; (b) 600 °C; (c) 800 °C; (d) 975°C.

Lattice parameters and misfit

The evolution of the lattice parameters for both phases, γ and γ′, with temperature is shown in Fig. 9. It is clearly visible that the lattice parameters of both phases γ and γ′ increase to different extents with rising temperature. The lattice parameters of the γ′ phase increase steadily, while the lattice parameters of the γ phase increase at a similar rate below 700 °C, but more rapidly afterwards than those of the γ′ phase. The corresponding misfit can be described as a function of the form $\delta = \delta_0 - Ae^{bT}$ as proposed in[25] and plotted in Fig. 10. In the equation, δ_0 is the misfit at room temperature, A and b are constants, and T is the absolute temperature. Between room temperature and 700 °C, the misfit waves for the three alloys stay almost constant at the value of the respective δ_0, due to the parallel and equal thermal expansion of the lattice parameters of both phases, γ and γ′. At temperatures above 700 °C, the more rapid increase of the γ lattice parameters relative to those γ′ phase results in a drastic decrease of the misfit[25]. It is notable that the misfit for all three alloys is always positive up to the dissolution of the γ′ precipitates.

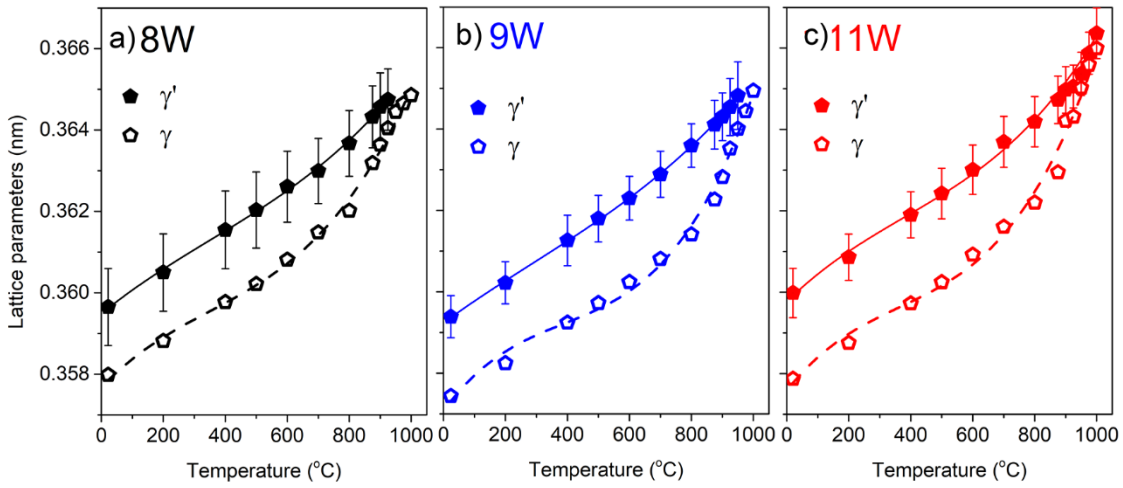

Fig. 9 Temperature evolution of lattice parameters for the phases γ and γ′ in the alloys 8W (a), 9W (b) and 11W (c); the lines represent fits with third order polynominals.

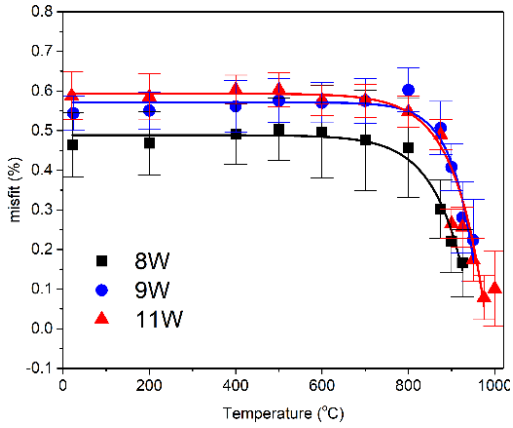

Fig. 10 Temperature dependence of the lattice misfit in the alloys 8W, 9W and 11W

It was reported for Ni-base superalloys that the increased thermal expansion of the γ phase lattice parameters can stem from the re-distribution of alloying elements between the γ and γ′ phases at higher temperature[25-27]. At lower temperatures, the lattice parameters of both phases γ and γ′ were only influenced by the thermal expansion[25]. In the Co-Al-W system, the elements Co and Al exhibit no significant partitioning preference between the γ and γ′ phase, while W strongly partitions to the γ′ precipitates at room temperature[4]. The change of lattice misfit with temperature, which is nearly independent of the temperature below 700 °C, can also be interpreted in light of the W partitioning behavior. Taking the fitting function into account, this means that the Ae^{bT} part is extremely small below 700 °C. However, with the temperature increasing towards the γ′solvus temperature, the γ′ precipitates dissolve releasing W atoms into the γ matrix[28]. The increasing content of W atoms in the γ matrix phase results in a rapid expansion of the γ lattice parameters. A change of the misfit partly induced by the re-distribution of the alloying elements between the phases γ and γ′ was also observed during the creep of the Co-28.8Ni-6.2Al-1.8Ti-2.0W-2.7Mo-1.8Nb-0.9Ta alloy[29]. As a result, a significant decrease of the misfit is observed at higher temperatures. The largest misfit in the low temperature range is found in 11W. But with the significant decrease of the lattice misfit above about 700 °C, the misfit values for the alloys 11W and 9W are nearly equal, as shown in Fig. 10. The misfit of alloy 8W is smaller by about 0.1% in the lower temperature range where the misfit stays nearly constant. The decrease of the misfit in alloy 8W is gentler than in the other two.

At the ageing temperature of 900°C, the γ/γ′misfit in 8W is the smallest, while in 9W and 11W the misfit valves are almost on the same level. It has been reported that in Ni-base superalloys with larger misfit, the γ′ phase prefers to align along <001> more regularly[29]. This is in agreement

with the observation in this study, as shown in Fig.1(a), the γ′ precipitates in 8W alloy are arranged more randomly. The misfit at ageing temperature also influences the morphology of the γ′ phase, as is well known for Ni-base superalloys. Coarsening γ′ precipitates attempt to transform from spheres to cubes during an ageing process due to the interfacial stresses induced by the misfit and the anisotropy of their elastic properties reducing those misfit induced stresses for interfaces aligned parallel to {100}. This tendency increases with increasing precipitate size [30,31]. Similar behavior of shape transition does also apply to these Co-Al-W alloys, as has been proven by the authors' earlier publication[3]. In other words, the finer particles exhibited a rounder shape due to the delayed shape transition even in two alloys with similar misfit. This should be the reason why the γ′ precipitates in the 9W alloy with smaller sizes were rounder than those in the 11W alloy, despite the similar misfit values in both alloys.

The different misfit measurements in this study are in accordance with certain other characteristics of the investigated alloys when taking into account the knowledge about misfit-property relationships in Ni-base superalloys. It is reported by some researchers that material with better creep strength always has a larger misfit[17,25,33]. But Rowland et al. argued that the volume fraction of the γ′ phase also plays an important role[34]. The creep behavior of the three alloys under investigation here was studied in an earlier paper[5] and, in deed, alloy 11W with the highest γ′ volume fraction and a misfit at least equal or slightly higher than in 8W and 9W at higher temperatures exhibited the lowest minimum creep rate.

Fig.11 shows the minimum creep rates of the three alloys at 850 °C under a load of 460 MPa[5] plotted versus the misfits at this temperature. It is obvious that the 8W alloy having the smallest misfit also exhibits the highest minimum creep rate indicating that it has the worst creep strength. However, the misfit of the 9W and 11W alloys are almost on the same level, while the creep strain rate of 11W is notably lower. This can be explained by the much higher volume fraction of the γ′ particles in the 11W alloy as well as the higher γ′ solvus temperature, that have been reported in the authors' earlier research[3,5], which also contribute to the better creep strength.

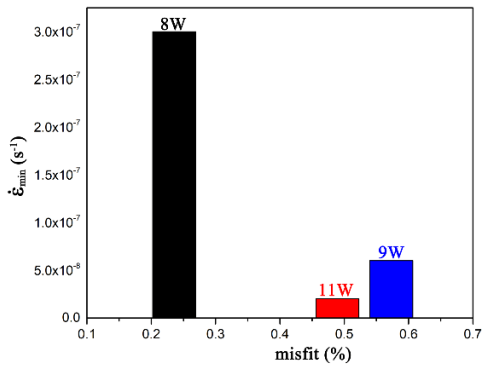

Fig.11 minimum creep rates of the three alloys under load of 460MPa at 850 °C, versus the misfits at 850 °C.

The misfit is likely to be effected by additional alloying elements, due to their complicated partitioning and re-distribution. This will briefly be discussed here based on some results published in literature about alloys with more complex compositions. It has been reported that, comparing to the Co-Al-W ternary alloys, the addition of Ni and Cr can decrease the γ/γ′ misfit by influencing the partitioning of W atoms between γ and γ′ phase[10,35]. On the contrary, the γ/γ′ misfit was increased to different extents by other additional alloying elements in order of Ta>Ti>Mo>V>Nb[10,36,37]. Surprisingly, the misfit of Co-Al-W-Ti/Ta alloys increased slightly with a rise in temperature[36,38], which is different to the situation of the ternary alloys as reported in the present work.

According to theoretical predictions in[39-41], materials with a large magnitude of misfit at temperatures below 750 °C and a small magnitude of misfit at higher temperatures should exhibit good creep resistance over any temperature range. Therefore, in case of these Co-Al-W-base alloys with positive misfit, the bigger magnitude at lower temperature and a smaller one at higher temperature, as shown in Fig.10, could provide advantages with respect to creep properties compared to Ni-base superalloys[38,42,43].

Conclusion

1) The lattice parameters of both γ′ and γ phases increase with rising temperature in a nearly parallel fashion before the γ′ precipitates start to dissolve. When the temperature rises above 700°C, the increase of the γ phase lattice parameter accelerates due to the re-distribution of W atoms from the dissolving γ′ precipitates.

2) The misfit valves approximately remain almost constant in the temperature range between 20 °C and 700 °C, but decrease drastically above 700 °C. Nevertheless, the misfit of these Co-Al-W alloys remains positive up to the γ′ solvus.

Acknowledgements

Dr. Yuzhi Li acknowledges the National Natural Science Fundation of China (51805308), the postdoctoral science foundation of China (2018M631189), the Natural Science Basic Research Plan in Shaanxi Province of China (2019JQ-303).

References

[1] Lee, C. Samuel. Precipitation-hardening characteristics of ternary cobalt-aluminum-X alloys. (Ph.D. thesis), The University of Arizona, Arizona, USA, 1971.

[2] J. Sato. Cobalt-base high-temperature alloys. Science. 2006, 312(5770): 90~91

[3] Y. Li, F. Pyczak, M. Oehring, L. Wang, J. Paul, U. Lorenz, Z. Yao. Thermal stability of γ′ phase in long-term aged Co-Al-W alloys. Journal of Alloys and Compounds. 2017, 729: 266~276

[4] F. Pyczak, A. Bauer, M. Göken, U. Lorenz, S. Neumeier, M. Oehring, J. Paul, N. Schell, A. Schreyer, A. Stark, F. Symanzik. The effect of tungsten content on the properties of $L1_2$-hardened Co-Al-W alloys. Journal of Alloys and Compounds. 2015, 632: 110~115

[5] Y. Li, F. Pyczak, J. Paul, M. Oehring, U. Lorenz, Z. Yao. Microstructure evolution in $L1_2$ hardened Co-base superalloys during creep. Journal of Materials Research. 2017, 32(24): 4522~4530

[6] Y. Li, F. Pyczak, J. Paul, M. Oehring, U. Lorenz, Z. Yao, Y. Ning. Rafting of γ′ precipitates in a Co-9Al-9W superalloy during compressive creep. Materials Science & Engineering A, 2018. 719: p. 43-48.

[7] F. Pyczak, B. Devrient, H. Mughrabi. The effects of different alloying elements on the thermal expansion coefficients, lattice constants and misfit of nickel-based superalloys investigated by X-ray diffraction. Superalloys 2004. 2004: 827~836

[8] F. Pyczak, S. Neumeier, M. Göken. Temperature dependence of element partitioning in rhenium and ruthenium bearing nickel-base superalloys. Materials Science and Engineering: A. 2010, 527(29-30): 7939~7943

[9] F. Pyczak, S. Neumeier, M. Göken. Influence of lattice misfit on the internal stress and strain states before and after creep investigated in nickel-base superalloys containing rhenium and ruthenium. Materials Science and Engineering: A. 2009, 510-511(18): 295~300

[10] L. Wang; M. Oehring, Y. Li, L. Song, Y. Liu, A. Stark, U. Lorenz, F. Pyczak. Microstructure, phase stability and element partitioning of γ-γ′ Co-9Al-9W-2X alloys in different annealing conditions, Journal of Alloys and Compounds, 2019, 787: 594~605

[11] C.T. Sims, N.S. Stoloff, W.C. Hagel. superalloys II. 1987,

[12] B. Marty, P. Moretto, P. Gergaud, J.L. Lebrun, K. Ostolaza, V. Ji. X-ray study on single crystal superalloy SRR99: Mismatch γ/γ′, mosaicity and internal stress. Acta Materialia. 1997, 45(2): 791~800

[13] S. Kraft, I. Altenberger, H. Mughrabi. Directional γ-γ′ coarsening in a monocrystalline nickel-based superalloy during low-cycle thermomechanical fatigue. Scripta metallurgica et materialia. 1995, 32(3): 411~416

[14] R. Gilles, D. Mukherji, M. Hoelzel, P. Strunz, D.M. Toebbens, B. Barbier. Neutron and X-ray diffraction measurements on micro- and nano-sized precipitates embedded in a Ni-based superalloy and after their extraction from the alloy. Acta Materialia. 2006, 54(5): 1307~1316

[15] R. Gilles, D. Mukherji, D.M. T Bbens, P. Strunz, B. Barbier, J. R Sler, H. Fuess. Neutron-, X-ray- and electron-diffraction measurements for the determination of γ/γ′ lattice misfit in Ni-base superalloys. Applied Physics A: Materials Science & Processing. 2002, 74: 1446~1448

[16] J.P. Collier, S.H. Wong, J.K. Tien, J.C. Phillips. The effect of varying AI, Ti, and Nb content on the phase stability of INCONEL 718. Metallurgical and Materials Transactions A. 1988, 19(7): 1657~1666

[17] F.R. Nabarro. Rafting in superalloys. Metallurgical and Materials transactions A. 1996, 27(3): 513~530

[18] G. Bruno, G. Schumacher, H.C. Pinto, C. Schulze. Measurement of the lattice misfit of the nickel-base superalloy SC16 by high-energy synchrotron radiation. Metallurgical and Materials Transactions A. 2003, 34(2): 193~197

[19] R. Gilles, D. Mukherji, M. Hoelzel, P. Strunz, D.M. Toebbens, B. Barbier. Neutron and X-ray diffraction measurements on micro- and nano-sized precipitates embedded in a Ni-based superalloy and after their extraction from the alloy. Acta Materialia. 2006, 54(5): 1307~1316

[20] J. Tiley, R. Srinivasan, R. Banerjee, G.B. Viswanathan, B. Toby, H.L. Fraser. Application of X-

ray and neutron diffraction to determine lattice parameters and precipitate volume fractions in low misfit nickel base superalloys. Materials Science and Technology. 2009, 25(11): 1369~1374

[21] P. Xu, S. Harjo, M. Ojima, H. Suzuki, T. Ito, W. Gong, S.C. Vogel, J. Inoue, Y. Tomota, K. Aizawab, K. Akita. High stereographic resolution texture and residual stress evaluation using time-of-flight neutron diffraction. Journal of Applied Crystallography, 2018, 51(3):746~760

[22] K.D. Liss, A. Bartels, A. Schreyer. High-Energy X-Rays: A tool for Advanced Bulk Investigations in Materials Science and Physics. Textures and Microstructures, 2003, 35(3-4): 219~252.

[23] B.B. Seth. Superalloys-the utility gas turbine perspective. Minerals, Metals and Materials Society/AIME, Superalloys 2000. 2000: 3~16

[24] K. Shinagawa, T. Omori, K. Oikawa, R. Kainuma, K. Ishida. Ductility enhancement by boron addition in Co-Al-W high-temperature alloys. Scripta Materialla. 2009, (61): 612~615

[25] Y.N. Gornostyrev, O.Y. Kontsevoi, K.Y. Khromov, M.I. Katsnelson, A.J. Freeman. The role of thermal expansion and composition changes in the temperature dependence of the lattice misfit in two-phase γ/γ′ superalloys. Scripta Materialia. 2007, 56(2): 81~84

[26] D. Siebörger, H. Brehm, F. Wunderlich, D. Möller, U. Glatzel. Temperature dependence of lattice parameter, misfit and thermal expansion coefficient of matrix, γ′ phase and superalloy. Zeitschrift Fuer Metallkunde/materials Research & Advanced Techniques. 2001, 92(1): 58~61

[27] R. Schmidt, M. Feller-Kniepmeier. Phase chemistry of a nickel-base superalloy after creep experiments. Scripta Metallurgica Et Materialia. 1993, 29(8): 1079~1084

[28] K. Shinagawa, T. Omori, J. Sato, K. Oikawa, I. Ohnuma, R. Kainuma, K. Ishida. Phase equilibria and microstructure on γ′ phase in Co-Ni-Al-W system. Materials Transactions. 2008, 49(6): 1474~1479

[29] J. Coakley, E.A. Lass, D. Ma, M. Frost, H.J. Stone, D.N. Seidman, D.C. Dunand. Lattice parameter misfit evolution during creep of a cobalt-based superalloy single crystal with cuboidal and rafted gamma-prime microstructures. Acta Materialia. 2017, 136:118~125

[30] M. Fährmann, P. Fratzl, O. Paris, E. Fährmann, W.C. Johnson. Influence of coherency stress on microstructural evolution in model Ni-Al-Mo alloys. Acta Metallurgica Et Materialia. 1995, 43(3): 1007~1022

[31] A.D. Sequeira, H.A. Calderon, G. Kostorz. Temporal Evolution of Bimodal Distribution of γ' Precipitates in Ni-Al-Mo Alloys under the Influence of Coherency Strains. Mrs Proceedings. 1995, 398: 483

[32] H. Mughrabi. Microstructural aspects of high temperature deformation of monocrystalline nickel base superalloys: some open problems. Metal Science Journal. 2009, 25(2): 191~204

[33] F.R. Nabarro, M.S. Duesbery. Dislocations in Solids-Vol 11. Amsterdam: Elsevier, 2002: 546~618

[34] L.J. Carroll, Q. Feng, J.F. Mansfield, T.M. Pollock. High refractory, low misfit ru-containing

single-crystal superalloys. Metallurgical & Materials Transactions A. 2006, 37(10): 2927~2938

[35] C.H. Zenk, S. Neumeier, N.M. Engl, S.G. Fries, O. Dolotko, M. Weiser, S. Virtanen, Mathias Göken. Thermophysical properties, creep and oxidation. Scripta Materialia, 2016. 112: 83~86

[36] H.Y. Yan, V.A. Vorontsov, J. Coakley, N.G. Jones, H.J. Stone, D. Dye. Quaternary alloying effects and the prospects for a new generation of Co-base superalloys. Superalloys 2012. 705~714

[37] C.H. Zenk, S. Neumeier, H.J. Stone, M. Göken. Mechanical properties and lattice misfit of γ/γ′ strengthened Co-base superalloys in the Co-W-Al-Ti quaternary system. Intermetallics, 55, 28~39

[38] H.Y. Yan, J. Coakley, V.A.Vorontsov, N.G. Jones,H.J. Stone, D. Dye. Alloying and the micromechanics of Co-Al-W-X quaternary alloys. Materials Science and Engineering: A, 2014, 613:201~208

[39] H. Biermann, M. Strehler, H. Mughrabi. High-temperature measurements of lattice parameters and internal stresses of a creep-deformed monocrystalline nickel-base superalloy. Metallurgical & Materials Transactions A. 1996, 27(4): 1003~1014

[40] J. Svoboda, P. Lukáš. Model of creep in 〈001〉 -oriented superalloy single crystals. Acta Materialia. 1998, 46(10): 3421~3431

[41] M.V. Nathal, R.A. Mackay, R.G. Garlick, M.V. Nathal, R.A. Mackay, R.G. Garlick. Temperature dependence of γ-γ' lattice mismatch in Nickel-base superalloys. Materials Science & Engineering. A. 1985, 1-2(75): 195~205

[42] H. Mughrabi. The importance of sign and magnitude of γ/γ′ lattice misfit in superalloys—with special reference to the new γ′-hardened cobalt-base superalloys. Acta Materialia. 2014, 81: 21~29

[43] H. Mughrabi, U. Tetzlaff. Microstructure and high-temperature strength of monocrystalline nickel-base superalloys. Advanced Engineering Materials. 2000, 2(6): 319~326